Review of Scientific Instruments ARTICLE scitation.org/journal/rsi

A solid-state, open-system, differential calorimeter

Cite as: Rev. Sci. Instrum. 91, 095102 (2020); doi: 10.1063/5.0013591
Submitted: 14 May 2020 • Accepted: 14 August 2020 •
Published Online: 2 September 2020

Shelby Lacouture,[1,a)] Trevor Dardik,[1] Dennis Van der Vliet,[2] Jephtah Akene,[3] Samuel Adeosun,[1] and Robert V. Duncan[1]

AFFILIATIONS

[1]Department of Physics and Astronomy, Texas Tech University, Lubbock, Texas 79410, USA
[2]Honeywell UOP, 50E Algonquin Rd., Des Plains, Illinois 60017, USA
[3]Southwest Research Institute, 6220 Culebra Rd., San Antonio, Texas 78238, USA

[a)]**Author to whom correspondence should be addressed:** shelby.lacouture@ttu.edu

ABSTRACT

This article details the design, modeling, construction, and evaluation of an open system calorimeter that operates in a normal room environment to measure endothermic or exothermic events in a system subjected to a steady heat flux. The calorimeter is unique because it allows the measurement of energy and power from an "open" system, where a heat flux enters and leaves the calorimetric boundary in a well-controlled manner. It is also novel because it utilizes a solid state heating and cooling assembly that acts as an electronic heat reservoir. The system is capable of measuring power levels from a few milliwatts to several watts, and it has been designed and optimized to be nearly immune to variations at ambient temperature and room airflow. The calorimeter was modeled using lumped parameter electrical–thermal equivalent circuits in SPICE software. This modeling in the electrical domain led to the use of a mathematical correction factor that mitigates mismatches in thermal conduction paths between an active and a passive cell as well as correcting differences in the sensitivities of the flux sensors employed for heat flow measurement. After obtaining a viable design, a prototype was constructed and validated with precise input power delivered via electric joule heating of a resistive element.

I. INTRODUCTION

Calorimetry has been employed for centuries as a means of measuring heat flow from systems contained within the calorimetric boundary. While calorimeters of even a few decades ago were relatively crude instruments, the application of modern technology, as well as an improved understanding of thermodynamics, has engendered extremely accurate, reliable instruments capable of measuring the flow and production of heat.[1]

While closed system, "bomb" type calorimeters are relatively simple and commercially available, these units require the experiment, or the sample, to be completely enclosed within the insulated region that defines the calorimeter, called the "calorimetric boundary," to accurately measure heat flow. The employment of calorimetry, however, has recently grown to encompass non-traditional uses, such as measuring the change in the rate of heat production from such sources as changes in the power losses in electronic equipment,[2–4] where more orthodox methods such as electrical signal capture fail to yield enough accuracy or resolution. Another example is in the biological fields: to quantify and to measure the change in the rate of heat released through metabolic processes in living organisms. Experiments such as these necessitate the use of an "open calorimeter," where a steady source of heat production, from electrical dissipation, gas and fluid flow, and potentially other sources, must be able to enter or leave the instrument. These open calorimeters detect very small changes in the rate of heat production within the calorimetric boundary as often much larger levels of heat flux through the boundary. Hence, an open calorimeter such as this is partially exposed to the outside environment in order to sustain this steady heat flux through the calorimeter. While all calorimeters must be able to reject perturbations from the external environment, this process is more demanding in an open calorimeter.

This paper details the design, construction, and evaluation of an open-system, differential calorimeter that operates in a normal,

room-temperature environment. The design uses a solid-state, proportional-integral-differential (PID) controlled cold-plate (CP) as a stable "heat reservoir," calibrated heat flux sensors, and a unique mathematical correction that greatly improves the common mode rejection (CMR) of the calorimeter to ambient temperature fluctuations. The inevitable mismatches that exist in thermal conductivity to ambient temperature, as well as mismatches within the active and passive components of the calorimeter, create systematic errors that may be readily characterized and corrected mathematically. The system is calibrated over an input power range of 5 mW to ~5 W and was compared to a prior open system differential calorimeter that was in use at the research facility before the development of this new design. The science of calorimetry is subtle and sensitive to systematic error sources, but the system and mathematical methods described herein are easily adapted to most calorimetric work and require few modifications to customize the calorimeter for many heat and power measurements.

II. OPEN SYSTEM DIFFERENTIAL CALORIMETER

A simplified diagram of the open system differential calorimeter is shown in Fig. 1. The calorimeter has two containers of an arbitrary shape (cylindrical in this case for the type of experiments performed at the facility where the system was designed), which are in good thermal contact with the top of their respective heat flux sensors (not visible in the image), while the other side of the sensors is connected to an active, electronically controlled cold-plate (CP). An experiment where heat or power output is to be measured is carried out in the active, or working, container, while the passive or reference container is filled with a substance/material that approximately mimics the heat capacity and thermal resistance of the active experiment. In concept, common environmental or instrumental fluctuations register on both the experimental and reference containers, so with proper sensitivity balance, these spurious fluctuations may be canceled by rejecting the common mode. Not shown in the figure is the thermal insulation that is placed around each respective container to eliminate ambient convective interference.

Each heat flux sensor develops a voltage output that is linearly proportional to the difference in temperature across its plates

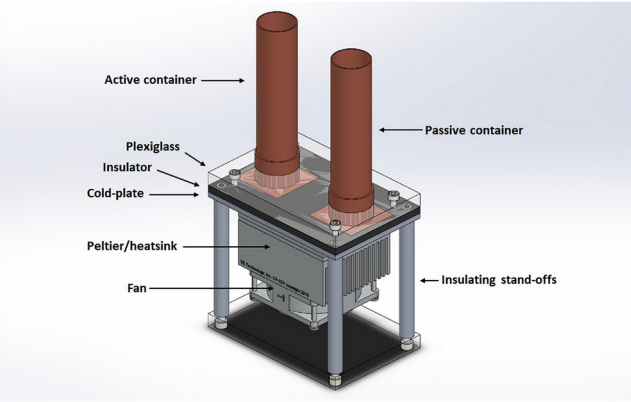

FIG. 1. 3-D rendering of the open system differential calorimeter.

(ΔT). The difference between the active and passive heat flux sensors is obtained and scaled to produce a signal that is proportional to the power evolved in the active container. The use of a passive container of roughly the same thermal characteristics as the active allows the subtraction of ambient temperature perturbations, in effect giving the system common mode rejection. This CMR is further enhanced by a symmetry factor acquired during initial calibration of the calorimeter – see Sec. III D. The individual components of the open system differential calorimeter are described in the following sections.

A. PID controlled solid-state cold-plate

The cold-plate used in the calorimeter acts as a uniform and stable variable-set-point temperature reference acting as a heat reservoir, which is able to sink or source heat without changes in its temperature. The system uses Peltier modules, with one side attached to the cold-plate and the other to a heatsink/fan. The specific cold-plate unit used is a model CP-200TT manufactured by TE technology, Inc., and the PID controller used is a model TC-720 from the same manufacturer. These units are capable of heating and cooling by operating the Peltier in a bipolar manner and are capable of achieving ±0.01 °C stability.

B. Heat flux sensors

Two types of technologies have been employed to measure heat flux ($\dot{Q}$) in the calorimeters discussed herein: Peltier modules and heat flux sensors (thermopiles). The original calorimeter design that the new system is based on used Peltier modules exclusively. The entropy of charge carriers changes as they flow across a junction of dissimilar metals, and this produces a heat flux that is proportional to the electrical current over a wide operational range. Given the resistivity of electrically conducting materials, this electrical current produces a voltage variation across the junction that is proportional to the heat flux through the junction. Peltier elements, which incorporate many junctions in parallel across the area of interest where the heat flux is to be measured, have not been specifically studied in-depth for use in this application. While their output voltage is seemingly linear over a given range of heat flux, they can show changes in sensitivity at differing absolute temperatures.[5] These devices also create their own ohmic power dissipation which, at adequately large heat flux, will cause clear departures from linearity. There are also large variations in sensitivity in this application, even among samples from the same supplier and lot. It is worth noting, however, that the sensitivities are usually an order of magnitude larger than those of equivalent-sized thermopiles. Peltier modules are also far less expensive than heat flux sensors.

For the reasons listed above (and anecdotal observations of a seemingly better signal to noise ratio), the calorimeter designed uses commercial heat flux sensors that are designed to compensate for these limitations that are intrinsic to Peltier junction arrays. These sensors were custom manufactured by FluxTeq, LLC and are based on their Ultra-09 model sensor. The units have nominal sensitivities of ~160 μV m^2/W. The custom-made units (designated as Ultra-01's) are smaller than the standard Ultra-09 model, being ~38 × 38 mm^2 squares, a size chosen to physically fit the current calorimeter's active and passive tube designs. A typical unit is shown in Fig. 2.

FIG. 2. Ultra-09 heat flux sensor.

C. Data acquisition

Data from the calorimeter were acquired with an Agilent model 34970A data acquisition unit. A 34901A 20-channel multiplexer card is used with the 34970A to capture all signals from the calorimeter and the live experiments performed. LabView software was chosen to implement interfacing with the 34970A and data collection and display via a graphical user interface (GUI).

III. LUMPED PARAMETER HEAT FLOW MODELING IN SPICE SOFTWARE

The open system differential calorimeter was studied using thermal lumped parameter electrical equivalent elements in LTspice software. Lumped parameter thermal modeling is a broadly employed method used to solve basic heat flow problems in many applications.[6,7] Its use in the development of the calorimeter described in this paper was not to determine absolute values for heat flow, temperatures, etc. It was rather used to ascertain the behavior of the system and the overall result of variations in ambient temperature and of mismatches in the thermal properties of the active and passive containers on the calculated output power. In this regard, the electrical equivalent modeling turned out to be a highly useful tool by producing a mathematical method for improving CMR.

A. Lumped parameter heat flow modeling

Lumped parameter electrical equivalent thermal element modeling is based on the similar mathematical relationships that exists between one dimensional conductive heat flow driven by a temperature gradient and one dimensional electric current flow driven by an electric potential gradient. The thermal relationship is expressed compactly by Fourier's law of heat conduction,

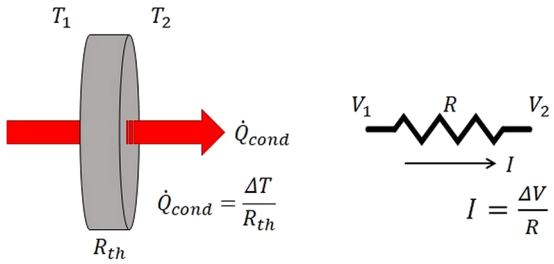

FIG. 3. Thermal–electrical analogy.

$$\dot{Q}_{cond} = -kA\frac{dT}{dx}. \quad (1)$$

Here, k is the thermal conductivity, and A is the area normal to the direction of the heat flow. Equation (1) is valid for the condition of $\dot{Q}_{cond}$ being constant, i.e., steady-state, which means the temperature gradient is also a constant. This leads to a simple relationship between the heat flow through a piece of material, the temperature difference developed across it, and the physical dimensions of the material that correlates nicely with the interrelationship between current, voltage, and resistance, respectively, as illustrated in Fig. 3.

Thermal resistance, much like electrical resistance, depends on the material (thermal conductivity) and the physical geometry through which heat conduction takes place. A similar electrical–thermal equivalent relationship exists for both convection and radiation of heat from the surface of a material, for which only the surface area of the material affects the equivalent lumped thermal resistance of a given shape. For the simulations performed in this paper, only convective heat transfer was included in the model. Convection is also a relatively strong function of temperature, and this effect is also included (as a linear function) in the SPICE model simulations.

There are likewise analogies for transient heat flow modeling using the concept of thermal capacitance as a lumped-parameter,[8] but this is only modeled roughly in the simulations performed for the calorimeter, and the time constant is scaled temporally to match the much faster paced simulations to the acquired data from actual experiments. If heat accumulated (Q) is of interest instead of the time rate of heat flow ($\dot{Q}$), there are quantitative ways of assessing the viability of using the thermal capacitance model to carry out transient analysis.[9] This would be useful in the transient analysis if the heat capacity of the two containers is mismatched. Our interest is primarily in the steady-state results, but time dependent, transient effects may be modeled in the lumped-element of SPICE as thermal capacitances.

B. Calorimeter heat flow modeling

To perform the thermal equivalent simulations for the calorimeter, both the experimental system (contained in the active tube) and the calorimeter itself are broken into segments that are approximately delineated by isotherms where heat flow can be considered one-dimensional. Again, the simulations were intended to observe system response to alter parameters and external perturbations; better absolute accuracy could be obtained by increasing the

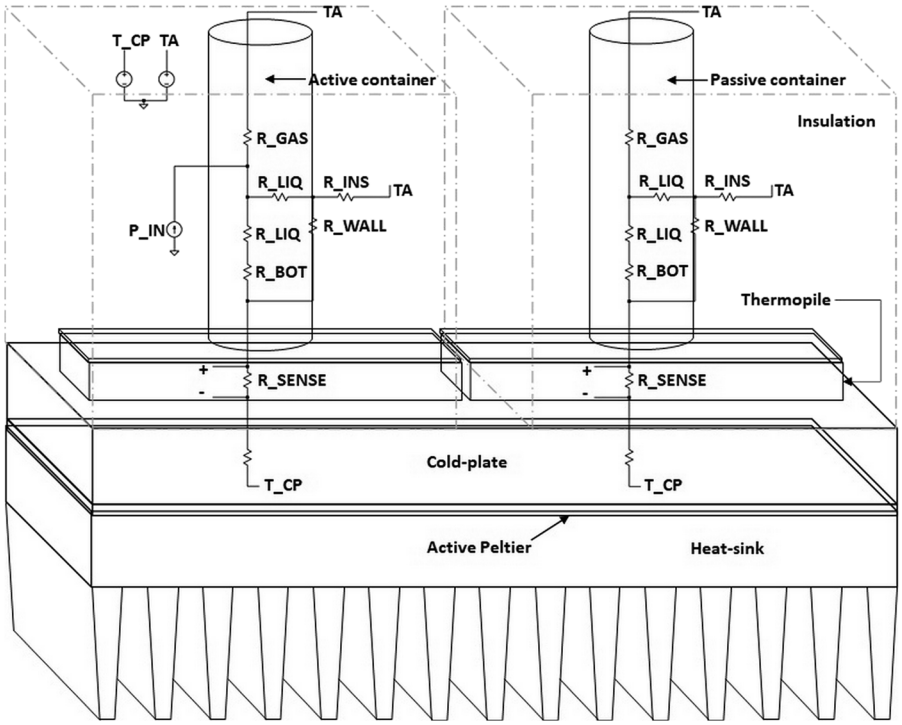

FIG. 4. Physical diagram with the electrical model overlaid.

number of elements corresponding to each physical segment. All simulations were performed in LTspice software. Figure 4 displays a diagram of the cold-plate differential calorimeter with the electrical simulation schematic overlaid to show the correspondence between the electrical components and their approximate corresponding physical segments.

The ambient temperature and the cold-plate set point are modeled as ideal voltage sources, and input power is modeled as an ideal current source. Heat flux sensors are simply modeled as resistors chosen so that the thermal resistance (°C/W) matches that of the physical flux sensor closely. The output of the heat flux sensors in the simulation is a temperature gradient (represented by a voltage in simulations) that is measured through the actual flux sensors' linear output in voltage per Watt heat flow (V/W). The sources can easily represent their physical counterparts; ambient can vary arbitrarily, mimicking room temperature swings, and the cold-plate source can be varied in a fast manner to imitate fluctuations in the PID during the active TE systems' temperature regulation.

C. Sample simulation result

An example simulation is illustrated in Fig. 5(a), alongside the data from a physical unit (b). The simulation shows a small (50 mW) step in input power and the corresponding waveforms from the flux sensors.

The slow, large swing seen in the output of the active and passive flux sensor signals is a variation in room temperature (TA source in the simulation), and the low-level, fast perturbations are from the control system of the cold-plate (CP source in the simulation). When the active and passive heat paths are closely matched

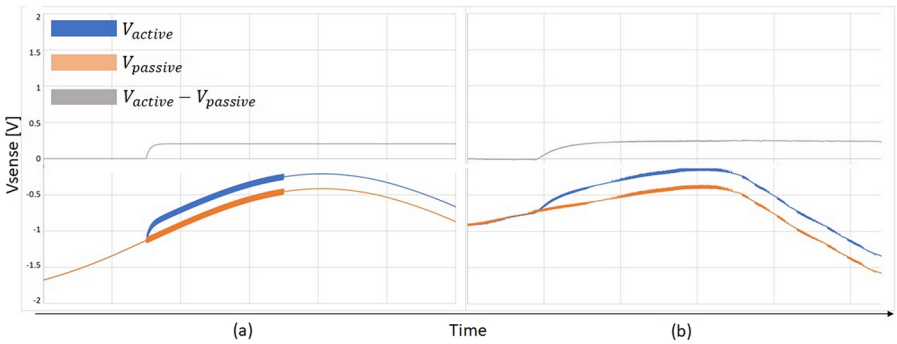

FIG. 5. Simulation vs data. The simulated data (a) and the actual sensor data (b) are shown, where the orange traces correspond to the reference sensor, and the blue traces correspond to the experimental sensor in response to a 50 mW step in input power.

(see Sec. III D), both of these unwanted signals are rejected in the difference signal, ΔV_{Sense}.

D. Symmetry errors and the mathematical correction factor

While the use of an active cold-plate as a heat reservoir and a stable reference improved the accuracy of the calorimeter both in simulations and empirically, another source of error in such an open system, as mentioned in Sec. III C, results from any asymmetry in the heat conduction and convection paths between the active and the passive containers to ambient temperature. This is easier to visualize if the entire simulation model for the calorimeter is dramatically simplified into an equivalent circuit that resembles an electrical Wheatstone-bridge circuit, as displayed in Fig. 6. This simplified analog model schematically shows how mismatched thermal resistance paths introduce errors; they cause a reduction in the differential circuits' CMR by altering the systems' symmetry.

In order to reject the common mode signal (ambient temperature in this case), the ratios of each branch's voltage divider (thermal paths in the physical system) must be equal,

$$\frac{R_{sense\_act}}{R_{sense\_act} + R_{loss\_act}} = \frac{R_{sense\_pass}}{R_{sense\_pass} + R_{loss\_pass}}. \quad (2)$$

This equality of ratios results in the magnitude of the signals from active and passive sensors to be equal for common-mode signals (ambient temperature). While it would be a physical impossibility to "trim" the thermal conduction and convection resistances, as well as perfectly match each flux sensor's sensitivity, a mathematical correction can be applied to the signal to regain good CMR in post-processing of the data. As a simple conceptual example, assume the left hand side (LHS) of Eq. (2) (active branch) evaluates to 0.5, but the right hand side (RHS) is 0.4 (passive branch). In this case, the CMR of the entire bridge is lost as the passive sensor develops only 80% of the active sensor's signal due to common-mode voltages (temperatures). If this imbalance could be determined quantitatively, the passive sensor output could simply be multiplied by a factor (1.25 in this particular example) to bring the passive signal magnitude back into equality with the active's and restore the CMR of the bridge circuit as a whole. In the electrical realm, this factor could be found by removing Q_in from Fig. 6, measuring both V_{active} and $V_{passive}$, and then dividing the former by the latter. As the voltage in each branch is proportional to the ratios in Eq. (2), their ratio gives the ratio of the RHS to the LHS and hence the needed restoration factor (1.25 in the preceding example).

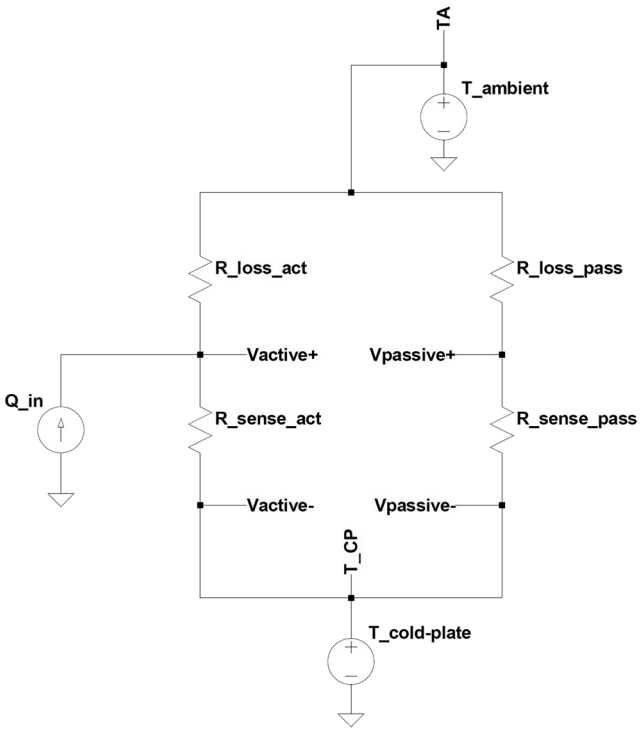

FIG. 6. Simplified equivalent circuit.

In the physical differential calorimeter, this restoration factor can be obtained as follows: a simple reading of each sensor is taken with no applied input power (Q_in set to zero in simulations), and the ratio of average V_{active} to average $V_{passive}$ over some finite time period is obtained. This correction factor is then used to mathematically bring the circuit back into "balance." The form of the corrected measured power signal then becomes

$$\dot{Q}_{measured} = C(V_{active} - \lambda V_{passive}). \quad (3)$$

Here, λ is the dimensionless empirically acquired correction factor, and C is a scaling factor in units of W/V. Figure 7 displays a simulation with the same temperature perturbation applied as in the previous simulations but where an intentional (large) asymmetry was introduced by increasing the passive container's convecting surface area to ten times that of the active side, in effect decreasing R_loss_pass, as shown in Fig. 6. Power input steps are gray, measured power out calculated without λ is the blue graph, and corrected power is the red graph.

As can be seen from the graph, the asymmetry caused by a larger convecting surface in the passive container leads to ambient temperature perturbations coupling into the measured output signal. The correction factor mathematically restores the ratios of the thermal conductance paths and hence restores the calorimeter's CMR. This dramatic improvement is obtained with the use of a simple initial measurement and a slightly altered $\dot{Q}_{measured}$ calculation.

The symmetry factor has been shown to be very effective in actual use; the graph in Fig. 8 displays the results of a calibration sequence (input power stepping) of a calorimeter where a large, fast swing at ambient temperature couples into the output measurement, resulting in a 50 mW (6.2%) variation in reading. The inset displays this erroneous original signal (blue graph) along with a corrected signal (black graph) that restores the calorimeter's CMR.

It should be noted that the idea of using a symmetry factor is not limited to the calorimeter described herein; the use of a corrective mathematical factor is viable in any differential system where access to each output is available, there are no phase shifts between the outputs, and a common-mode signal can be applied without a concurrent differential-mode signal.

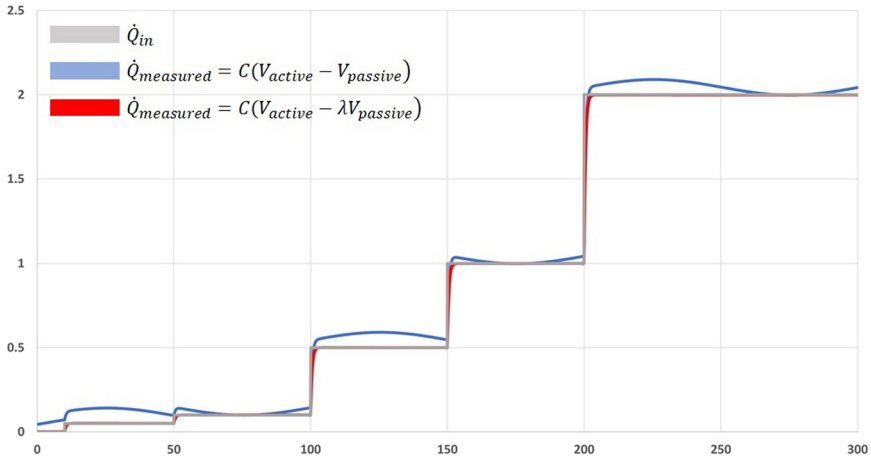

FIG. 7. Intentional asymmetry and the corrected signal.

IV. RESULTS

The following sections cover the physical evaluations and simulations of the cold-plate differential calorimeter, with comparisons to the passive heatsink-based calorimeter which preceded the active heat sink CP design.

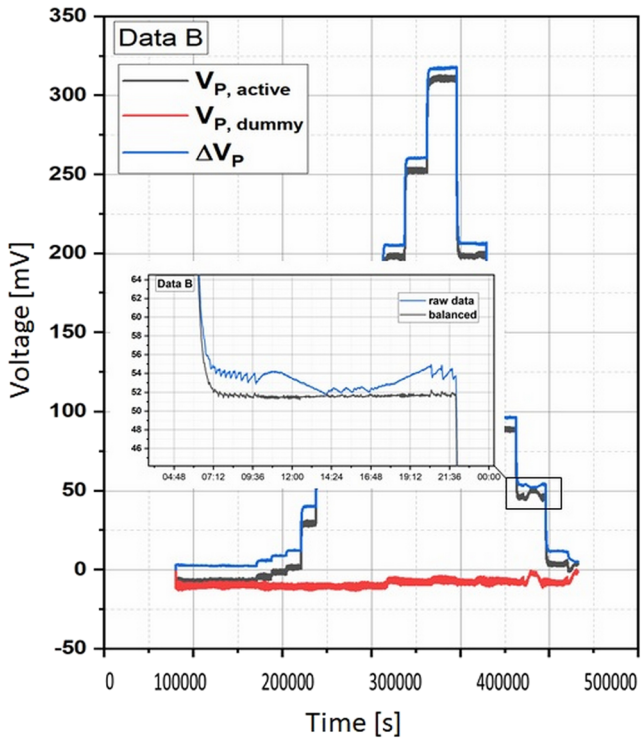

FIG. 8. Ambient perturbation and correction via a symmetry factor.

A. Heatsink calorimeter evaluation

As stated in the Introduction, the calorimeter is an improved design based on a prior differential calorimeter. The prior calorimeter utilized a simple heatsink instead of the active cold-plate technology described above, incorporating thermoelectric Peltier modules to measure the heat flow instead of the improved heat flux sensors. It was observed experimentally that the passive calorimeter design would show fluctuations in measured output power with variations in ambient temperature and calibration factors (calculated by applying power step sequences) would change if the calorimeter was used at a different average ambient temperature than that used during calibration. This can be mostly attributed to two factors: (1) mismatches in thermal conduction through loss paths (any path other than directly through the flux sensing element) and sensing elements between active and passive, as described in Sec. III D, and (2) variations in convection from the heatsink to ambient. The first can simply be fixed by the use of the symmetry factor described in the prior section, while the second effect cannot be mitigated mathematically due to the inherently non-linear (and hence unpredictable)

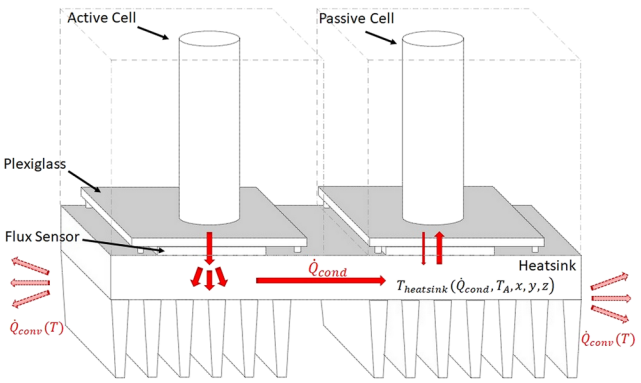

FIG. 9. Main heat flow paths through the heatsink calorimeter.

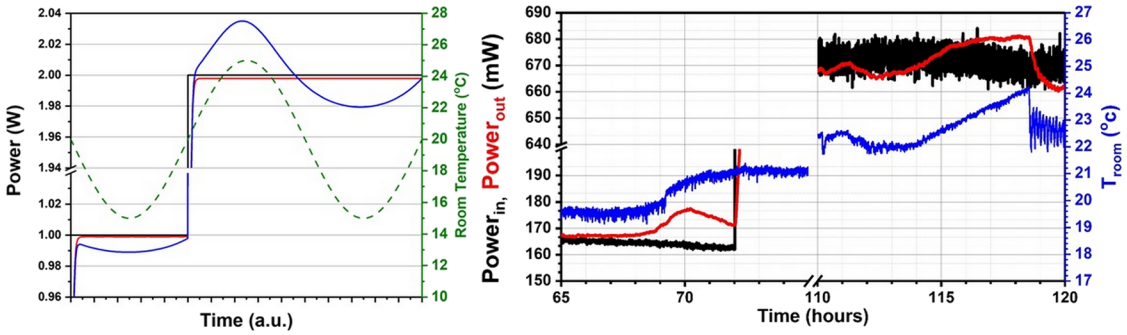

FIG. 10. Errors due to non-linear heat ejection: (a) simulated data and (b) actual sensor data.

nature of convection. Figure 9 displays the most prominent heat flow paths through the prior passive heatsink type of differential calorimeter.

While heat conduction is a relatively weak function of temperature, convection is a strong function of temperature, and the air flow impinging upon the surface through convection is unpredictable. As pointed out in the diagram of Fig. 9, the local temperature of the heatsink is a function of heat flow, ambient temperature, and spatial position (x,y,z). This leads to varying heat flow to ambient through the heatsink at different points on the surface that cannot be accounted for in a scaling factor due to this unpredictable convective non-linearity. The variation in this convection from the heatsink calorimeter was easily seen in the SPICE modeling of the old design; changes in the convection of the heatsink altered the thermal symmetry of the system at different average temperatures. This was one of the main reasons for employing the CP technology in the new design. Figure 10(a) displays the simulated response of the new and old designs with discrete power steps applied in the presence of a ±5 °C temperature swing centered at 20 °C. The simulations were run with both active and passive heat paths exactly matched. Even with this close matching of containers and sensors, the measured output power from the passive heatsink calorimeter (blue graph) gives false values due to a mismatched convective heat transfer coefficient caused by the localized heating of the heatsink compared to the input power steps (black graph). The new active cold-plate calorimeter output (red graph) is unperturbed by these fluctuations at ambient temperature. Figure 10(b) displays this phenomenon in data from an actual heatsink calorimeter; the measured output power (red graph) closely follows the ambient temperature variations (blue graph) once the heatsink warms up enough to appreciably alter the convection and ultimately conduct from the sensing element to ambient.

Another issue with passive heatsink systems was a rather large flow of heat from the active to the passive cell through the heatsink. This effect is visible in the simulations of this type of calorimeter, Fig. 11(a), and in actual data, Fig. 11(b), where the passive signal

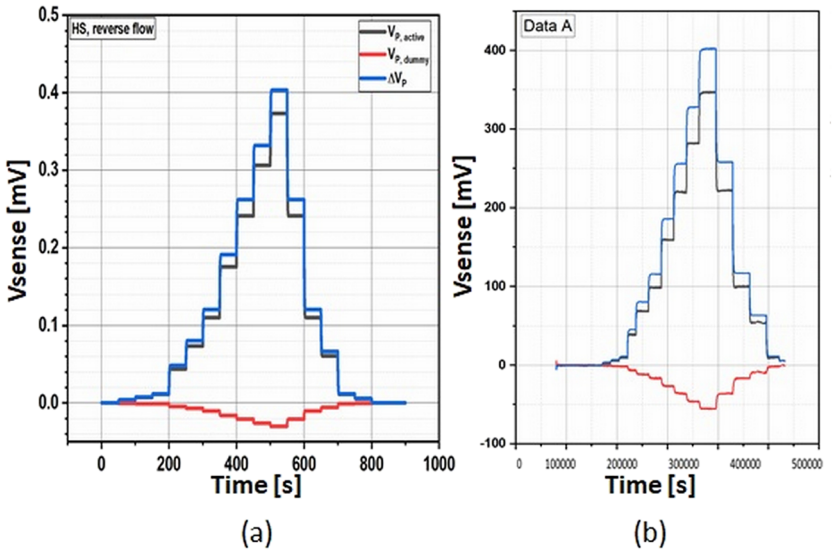

FIG. 11. (a) Empirical and (b) simulation calibration signals of the heatsink calorimeter.

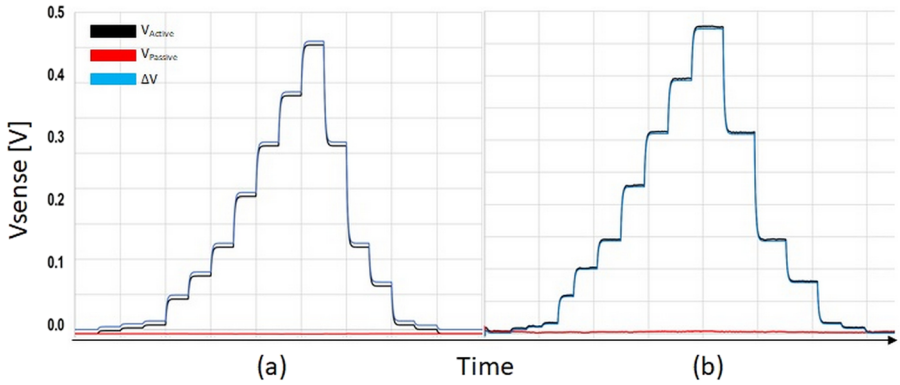

FIG. 12. (a) Simulated and (b) actual calibration signals of the cold-plate calorimeter.

(red graph) can be seen swinging in reverse, matching the reverse energy flow.

B. Cold-plate calorimeter evaluation

The errors pointed out in the last section were the impetus for the redesigned calorimeter employing the active CP technology to function as a virtual heat reservoir. This improvement, coupled with the development of the symmetry factor, has effectively eliminated the aforementioned errors, producing a calorimeter that is highly accurate, even in poorly controlled laboratory environments. Figure 12 displays the results of a calibration sequence simulated in LTspice software, Fig. 12(a), and actual empirical data, Fig. 12(b). The reverse heat flow is no longer present, and CMR is exceptional with the use of closely matched heat flux sensors and the additional use of the symmetry factor.

An example calibration result is shown in Fig. 13; the sequence of input power steps, illustrated in Fig. 12, is used to form a best-fit line, the slope of which gives the static calibration factor C (W/V), and this factor, along with the symmetry factor, is then used in active runs for that particular calorimeter to calculate the measured output power.

Figure 14 displays the divergence from the calibration line for each power step for the calorimeter, both with and without the symmetry factor applied.

This graph nicely points out the efficacy of the symmetry factor; mismatched thermal pathways are dramatically mitigated with this factor applied. The graph also nicely displays the calorimeter's uncertainty over a range of power from 5 mW input to ~5 W. Up to ~4 W, the excursions from zero power are less than 1%. The large divergence as power goes well beyond the 4 W level is due to convection and radiation losses becoming a larger percentage of the power input; this is equivalent in the electrical analogy to R_{Loss}, shown in Fig. 6, becoming smaller, with a concomitant shift in some of the heat flowing away from the heat flux sensor and out to ambient.

In order to characterize the calorimeter's response in a normal room-temperature environment, several power steps were applied for relatively long periods of time with each step lasting at least 24 h. Figure 15 shows the results of this study; the input electrical power was stepped through approximately 5 mW, 115 mW, 125 mW, 480 mW, and 505 mW power levels. The small steps were

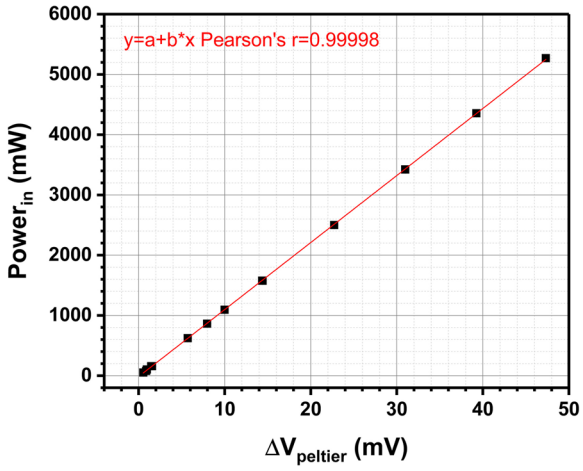

FIG. 13. Example calibration for the cold-plate calorimeter.

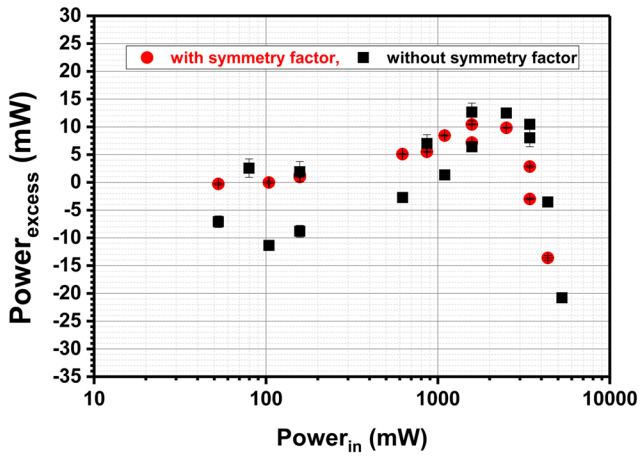

FIG. 14. Distribution of power steps around the linear-fit.

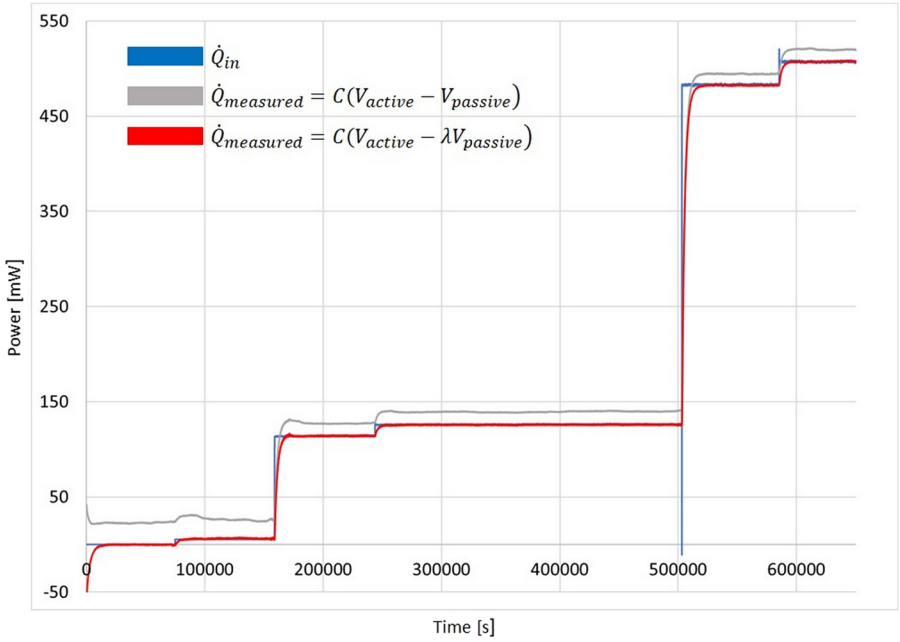

FIG. 15. Power step series on the calorimeter.

intended to qualify the calorimeter's ability to detect small power deviations. Again, while this calorimeter was well-matched in terms of cell and sample size and mass and while the flux sensors were chosen with closely matched sensitivities, the symmetry factor nicely corrected the measured output signal visibly, as can be seen by the offset and room perturbations displayed in the uncorrected signal (gray).

The smallest step, at 5 mW, is shown close-up in Fig. 16. It is hard to infer much from the raw, scaled $C\Delta V_{Sensor}$ signal, but the step is steady and measurable with the mathematical correction applied. Note that the downward "spike" in Q at T = 500 000 is due to a momentary loss of input from the power supply.

Numerically, the input power was averaged to be 5.31 mW, and the output power was averaged at 6.27 mW with a peak to peak

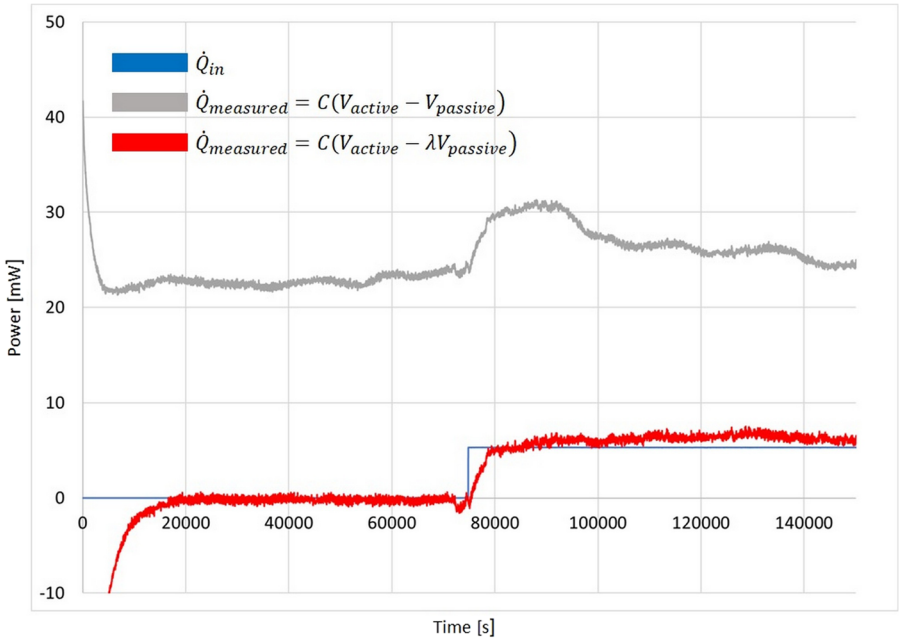

FIG. 16. 0 mW–5 mW step.

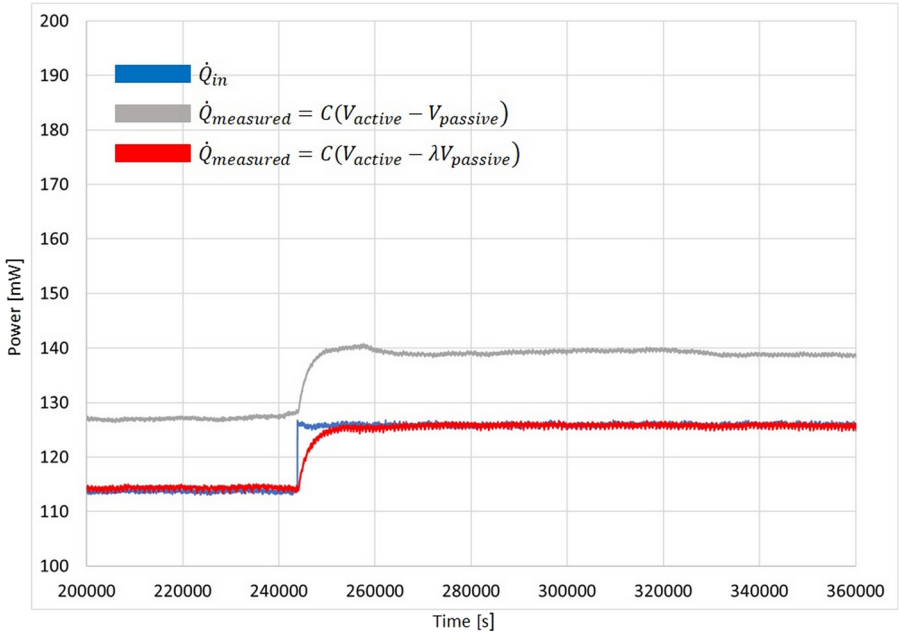

FIG. 17. 115 mW–125 mW power step.

(pk–pk) deviation of 2.29 mW. The step from 115 mW to 125 mW is shown in Fig. 17; the 10 mW jump is quite steady in the measured output, even through a day–night cycle. Numerically, the average input power was 125.9 mW, as the output power averaged 125.8 mW with a measured noise of 1.78 mW pk–pk. It should be mentioned that the noise of the supply was comparable in this power regime, measuring 1.74 mW pk–pk.

V. FUTURE WORK

While the differential calorimeter described in this article has proven to be highly accurate and reliable for measuring power from various materials and physical systems, several modifications are going to be evaluated in the near future for potential improvements to the system's accuracy, sensitivity, and noise immunity. One potential modification is extending the cold-plate from the base to a "shield" mostly covering the active and passive containers. This shielding will create an isotherm around the containers and further mitigate the transfer of heat to or from ambient room temperature. Another minor improvement could be the addition of more heat flux sensors placed around the extended CP shield. This addition of an array of sensors would have to be calibrated since each sensor has a slightly varying sensitivity. We are also planning to conduct experiments that are designed to measure how much heat can escape the calorimeter in paths other than the primary conduction path through the heat flux sensor. This characterization is dependent upon the geometry and thermal anchoring of the sample under test. Accurate measurements of the low-level of heat transfer through these unintended heat pathways will allow us to quantitatively determine the small systematic errors associated with these calorimetric measurements, but many only take place after each sample is installed.

VI. CONCLUSION

An open-system, differential calorimeter designed to be used in normal room environments was designed and tested. The system was simulated using thermal lumped-parameter electrical equivalent circuit analysis. The electrical equivalent circuit modeling led to the adoption of a symmetry factor that compensates for any mismatches in heat flow between an active and a passive container and for mismatches in the sensitivities of the flux sensing elements used to measure heat flow.

The differential calorimeter has been shown to have precision and accuracy within 1% over a range from 5 mW up to and slightly above 4 W, with a resolution of ~1 mW over this range of operation. The system can be easily adapted to measure energy or power from experiments contained in arbitrarily shaped "cells," and it may be operated in a standard room or laboratory environment; hence, it does not require a temperature-controlled environment to operate accurately.

ACKNOWLEDGMENTS

This work was sponsored in part by Seashore Research Laboratory, LLC and by the State of Texas TRIP Program. The authors would like to thank Alison Godfrey for her leadership and contributions. Her help was essential in establishing the environment in which this research was conducted and development effort was made.

DATA AVAILABILITY

The data that support the findings of this study are available from the corresponding author upon reasonable request.

REFERENCES

[1]S. Sarge, G. Höhne, and W. Hemminger, *Calorimetry* (Wiley VCH, Weinheim, Germany, 2014).
[2]K. J. Bradley, A. Ferrah, R. Magill, J. C. Clare, P. Wheeler, and P. Sewell, "Precision calorimetry for loss evaluation," in *IEE Half Day Colloquium on Testing of Electrical Machines (Ref. No. 1999/161)* (IET, Nottingham, UK, 1999), pp. 3-1–3-3.
[3]P. Wolfs and L. Quan, "Precision calorimetry for power loss measurement of a very low power maximum power point tracker," in *2007 Australasian Universities Power Engineering Conference* (IEEE, Perth, WA, 2007), pp. 1–5.
[4]J.-P. Keradec, "Validating the power loss model of a transformer by measurement—Validation is key," IEEE Ind. Appl. Mag. **13**(4), 42–48 (2007).
[5]T. Haruyama, "Peltier heat flux sensor for cryogenic use," in *Advances in Cryogenic Engineering. Advances in Cryogenic Engineering*, edited by Q. S. Shu (Springer, Boston, MA, 2000).
[6]Y. Cengel, A. Ghajar, and M. Kanoglu, *Heat and Mass Transfer* (McGraw-Hill, Tamil Nadu, India, 2016).
[7]A. Mills, *Basic Heat and Mass Transfer* (Prentice-Hall, Upper Saddle River, NJ, 1999).
[8]F. Incropera, *Principles of Heat and Mass Transfer* (Wiley, Hoboken, NJ, 2013).
[9]N. Ukrainczyk and S. Sabo, "Laboratory made differential calorimeter to study cement hydration," in MATRIB 2011 International Conference on Materials, Tribology, and Recycling, 2011.